On the Use of Knitted Antennas and Inductively Coupled RFID Tags for Wearable Applications

Damiano Patron, *Member, IEEE*, William Mongan, *Member, IEEE*,
Timothy P. Kurzweg, *Senior Member, IEEE*, Adam Fontecchio, *Senior Member, IEEE*,
Genevieve Dion, Endla K. Anday, and Kapil R. Dandekar, *Senior Member, IEEE*

Abstract—Recent advancements in conductive yarns and fabrication technologies offer exciting opportunities to design and knit seamless garments equipped with sensors for biomedical applications. In this paper, we discuss the design and application of a wearable strain sensor, which can be used for biomedical monitoring such as contraction, respiration, or limb movements. The system takes advantage of the intensity variations of the backscattered power (RSSI) from an inductively-coupled RFID tag under physical stretching. First, we describe the antenna design along with the modeling of the sheet impedance, which characterizes the conductive textile. Experimental results with custom fabricated prototypes showed good agreement with the numerical simulation of input impedance and radiation pattern. Finally, the wearable sensor has been applied for infant breathing monitoring using a medical programmable mannequin. A machine learning technique has been developed and applied to post-process the RSSI data, and the results show that breathing and non-breathing patterns can be successfully classified.

Index Terms—Antennas, biomedical communication, RFID tags, textile technology, wearable sensors.

I. INTRODUCTION

RECENTLY, the integration of wireless smart devices into clothing has revolutionized the monitoring of physical activities and wellness. These garments incorporate physiological sensors and low-power computing units allowing for continuous biomedical monitoring and activity tracking [1], [2]. By adding low-power transceivers, such as Bluetooth Low Energy devices (BLE), the information can be conveniently transmitted to mobile devices. However, these devices typically use additional dedicated transceiver modules and require batteries or other sources of energy.

Radio-Frequency Identification (RFID) technology is being increasingly utilized in an expanding set of applications. For traditional metal-based tags, it has been shown that the backscattered power (RSSI) transmitted from a passive RFID tag can be used as metric for detecting material deformations [3]. In other words, when a strain force is applied on an RFID tag, the physical deformation of the embedded antenna causes a shift of its resonant frequency. Consequently, the RSSI variation received from the interrogator can be correlated to the mechanical deformation of the object where the tag is installed.

In this paper, we propose to take advantage of this new application of RFID technology, along with advances in knitting-based fabrication techniques, to realize comfortable and battery-less wearable strain sensors. These sensors can be used for monitoring contractions, respiration patterns and limb movements. In other words, these sensors can be used for applications where a mechanical movement causes stretching and changes in RSSI responses. As a result, the desired wearable wireless strain sensor should meet the following requirements: 1) comfortable to wear, 2) highly stretchable, 3) good impedance matching between antenna and microchip, and 4) sufficient radiating characteristics to maintain communication under different levels of physical deformation.

The feasibility of building electrical devices using conductive fabrics has been analyzed through electrical characterization of transmission lines [4]. Several papers have demonstrated mounted wearable transmission lines and antennas where conductive fabrics are applied onto woven fabrics [5]. Previous work shows conductive copper foil or fabrics bonded to a flexible substrate. These techniques show limitations in terms of electrical losses and bulkiness. We address these drawbacks by knitting conductive and non-conductive yarns in a single process, resulting in smart textiles that are unobtrusively integrated into the host garment, eliminating the need for chemical adhesives that degrade performance and decrease elasticity.

The proposed wearable strain sensor is composed of a folded dipole antenna, equipped with an inductively coupled RFID tag. As opposed to conventional microchips, the two small pads of the RFID chip package do not require physical soldering to the antenna arms as the energy is inductively transferred through an internal matching circuit. The advantage of this inductively

D. Patron, T. P. Kurzweg, A. Fontecchio, and K. R. Dandekar are with the Department of Electrical and Computer Engineering, Drexel University, Philadelphia, PA 19104 USA (e-mail: damiano.patron@gmail.com; kurzweg@coe.drexel.edu; afontecchio@coe.drexel.edu; dandekar@coe.drexel.edu).

W. Mongan is with the Department of Computer Science, Drexel University, Philadelphia, PA 19104 USA (e-mail: wmm24@drexel.edu).

G. Dion is with the Westphal College of Media Arts and Design, Drexel University, Philadelphia, PA 19104 USA (e-mail: gd63@drexel.edu).

E. K. Anday is with the College of Medicine, Drexel University, Philadelphia, PA 19104 USA (e-mail: endla.anday@drexelmed.edu).

Color versions of one or more of the figures in this paper are available online at http://ieeexplore.ieee.org.

Digital Object Identifier 10.1109/TBCAS.2016.2518871

coupled RFID technology is in maintaining the full flexibility of the fabric, even around the microchip area. Furthermore, under sufficiently large mechanical deformations, the RSSI variation will be enhanced by the decoupling between the microchip and the antenna's arms.

The ability to determine aberrations in the control of respiration using RFID technology may have particular importance in detecting apnea, or cessation of respiration. Monitoring infants at risk for respiratory events could be helpful in detecting apnea which, if not reversed in a timely manner, could lead to cardiorespiratory arrest. Currently, the technology for monitoring infants at risk involves equipment that is connected by cables attached to two electrodes on the baby's chest under his or her arms. As the baby's chest moves during breathing, the impedance between the electrodes changes. If the monitor does not detect changes in the electrodes triggered by a baby's breathing effort, a light will come on and an alarm will sound. However, these monitors are bulky, require frequent recharging, and are prone to signal interference that can occur from external sources; interference could cause the monitor to miss apnea with resultant respiratory arrest. In the field of contactless respiration sensors, in [20] the authors propose a system-on-chip UWB pulsed radar for respiratory rate monitoring. In [21] the authors propose the design of an integrated circuit equipped with a MEMS sensor for measuring the patient's nasal air flow, which require an on-board cell battery.

The wearable strain sensor described in this paper has the potential for improving these current technologies since it can be used to wirelessly detect breathing pattern with a comfortable and battery-less garment, using commercial off-the-shelf components. In order to evaluate the performance of the strain sensor for apnea monitoring, we have used a mechanical baby mannequin which is used for medical training. This mannequin, called Laerdal SimBaby [13], can be programmed with specific breathing and non-breathing intervals and the chest of the baby resembles the usual expansion of a breathing pattern. These intervals are classified using real-time statistical processing approaches, including Support Vector Machines, FFT, and hypothesis testing, some of which have been used successfully in analyzing electromyogram signals in the past [17]. In this paper we show that the proposed sensor, along with a machine learning algorithm for post processing the RSSI data, is able to successfully classify the breathing or non-breathing patterns using a Support Vector Machine, classifying on statistical features of that RSSI data as well as accurately estimate the rate of breathing of the subject. In Fig. 1 we show a diagram of the full system comprising the wearable sensor and the RFID receiving system.

This paper is organized as follow: in Section II we discuss the textile material selection and characterization, the RFID tag, and the simulation of the folded dipole antenna. Section III describes the measurement results in terms of the antenna input impedance and radiation characteristics, and quantifies human body proximity effects on RFID sensor performance. In Section IV we analyze the system level performance when the sensor is employed for respiration monitoring. Finally, conclusions are drawn in Section V.
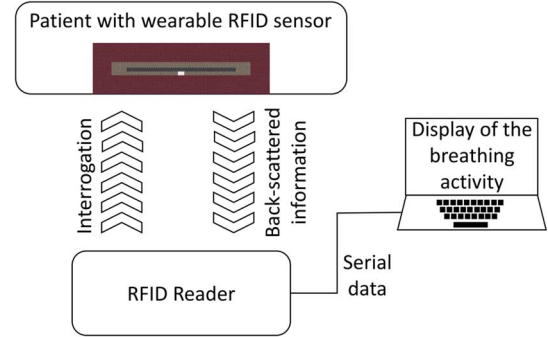

Fig. 1. Block diagram of the full system. The RFID reader interrogates the wearable sensor, which responds with RSSI values that vary based on the level of stretching. The RSSI data are transferred to the computer for the machine learning processing and final display of the breathing activity.

TABLE I
SUPPORTING MATERIALS CHARACTERISTICS

Material	ε_r	*Tan(δ)*
Polyethylene Foam	1.2	0.01
Mix of Woll and Lycra	1.5	0.03

II. WEARABLE RFID STRAIN SENSOR DESIGN

A. Material Selection and Characterization

The strain sensing application of the proposed knitted RFID tag requires a high degree of flexibility under mechanical deformation. For the non-conductive part of the garment, we employed a mix of wool and lycra, which maintains the planar antenna architecture while ensuring high elasticity. The conductive layout was knitted with high conductive, silver-coated yarns. As a substrate support for non-human body based laboratory measurements, we used a 55 mm thick polyethylene foam having a dielectric constant close to air.

For accurate simulations of the antenna design, we characterized the non-conductive fabric as well as the foam support through an Agilent 85070E Dielectric Probe Kit connected to a N5230A Vector Network Analyzer. The measurement estimates the dielectric constant, or complex permittivity $k = \varepsilon_r = \varepsilon_r' - j\varepsilon_r'$, as well as the $Tan(\delta) = \varepsilon_r''/\varepsilon_r'$. While the former measures how much energy is stored in a material, the latter expresses how lossy or dissipative the material is. Table I summarizes the measured characteristics. The dielectric constant of the foam approximates the unitary value of the air, whereas the non-conductive textile is slightly higher. For both materials, the loss tangent is relatively low.

For knitting the conductive layout, we selected a 99% pure silver plated nylon yarn having linear resistance equal to 50 Ω/m and 27% of maximum elongation. When a conductive yarn is used, the finite conductivity of the planar structure is determined by the yarn's linear resistance and knitting method. As the contact area between the conductive loops increases, the equivalent resistance of the fabric decreases. Furthermore, the conductivity is highly dependent on the direction of the current flow in the textile, knitting geometry and loop density [6].

To ensure good conductivity of the overall design, the loops forming the antenna are tightly knit, even when the fabric is in a relaxed state. In Fig. 5(c) we show a close-up picture of the knitted pattern. The conductive threads have been made denser along the direction of maximum current flow, in order to minimize the conduction losses. The following antenna layout selection and optimization takes into account the aforementioned factors as well as the practical manufacturability using conventional knitting machines for industrial production.

B. RFID Tag Selection

One of the major challenges of smart textiles is the integration of lumped components, which require physical connection with the conductive textile element. In the literature we can find several approaches that attempt to address this challenge [6]. However, the use of conductive epoxy and other solid compounds tend to stiffen the structure and degrade the electrical performance.

We addressed this limitation by utilizing a novel approach. We selected the Murata MAGICSTRAP, a 2-port IC tag employing inductive coupling technology [7], as an RFID tag for the wearable strain sensor. Specifically, the two small pads of the SMD component allow coupling of the RF energy to the two antenna's arms, avoiding the need for physical soldering. The component can be easily integrated into textiles by knitting a small pocket between the two antenna arms, thus maintaining the full flexibility and comfort of the resulting garment. Furthermore, this choice allows for enhancing the strain sensitivity to physical deformation, as joint variations of input impedance and RF decoupling are significantly higher than radiation pattern changes alone [3]. In other words, by using the proposed RFID tag, the physical deformation of the antenna causes impedance variations and coupling reduction between the IC and the antenna, yielding significant variations of the backscattered power (RSSI).

For the above reasons, we selected the MAGICSTRAP model LMXS31ACNA-011, a small 3.2×1.6 mm SMD IC with input impedance equal to $Z_c = 25 - j200\ \Omega$ within the 870–915 MHz frequency bandwidth. In Table II we summarize the main features of the RFID tag. The SMD package includes a standard EPC global Class1Gen2 integrated circuit, along with a matching unit that allows the inductive coupling of energy between the component's pads and the knitted antenna. When considering the practical washability of the final garment, the component can sustain up to 150°C for 2 hours, which makes it suitable for standard laundry processes. The high ESD (system-level electrostatic discharge) protection function makes it safe and compatible for wearable applications.

C. Knitted Antenna Design

Typically, the input impedance of RFID tags $Z_c = R_c + jX_c$ does not match with the 50 Ω standard which characterize the majority of front-end antennas. Due to the non-zero reactance X_c, antennas for RFID tags are properly designed for complex conjugate matching with these unconventional impedances. For the case of the MAGICSTRAP RFID tag, the input impedance is characterized by a resistance $R_c = 25\ \Omega$ and a reactance of $X_c = -200\ \Omega$.

TABLE II
MAGICSTRAP IC CHARACTERISTICS

Input Impedance	$Z_c = 25 - j\ 200\ \Omega$
Frequency	870 – 915 MHz
Dimension	3.2 x 1.6 x 0.55 mm
EPC Memory	240 bits
User Memory	512 bits
TID Memory	64 bits

Because of the negative values of X_c, the proposed antenna topology was selected to exhibit inductive reactance for complex conjugate matching and thus maximum energy delivery between the microchip and the antenna. For this reason, we chose to design a folded dipole antenna, which has two major characteristics that align with system requirements. First, the loop structure in the knitting process allows us to achieve positive reactance for proper complex conjugate matching with the RFID tag. Second, the simple planar layout makes the folded dipole architecture suitable for conventional knitting machines while allowing alignment of the conductive thread along the direction of maximum current flow.

When designing knitted or embroidered conductive structures, the layout cannot be modeled or assumed to be a pure conductive sheet. In our case, we can define knitting as the process of creating fabric with yarns by forming a series of interconnected loops. As suggested in [8], these structures exhibit higher electrical length compared to corresponding ideal copper sheets. For these reasons, the conductive layout should be modeled by a sheet impedance Z_s comprising resistive and imaginary parts and expresses in Ω/sq. While the resistance accounts for the ohmic losses, the imaginary part contributes to the antenna input reactance due to the electrotextile knitted loops.

The antenna was modeled and simulated with the High Frequency Structure Simulator (HFSS). The design is a folded dipole with a thin slot whose width and length act as the main tuning parameters for impedance matching at 870 MHz. The complex sheet impedance was determined through a series of parametric simulations and comparison with a measured prototype. The best fit between measurements and simulations was achieved when $Z_s = 0.2 - j2.6\ \Omega/\text{sq}$. Fig. 2 shows the 3D antenna model for numerical simulations, where the antenna layout is placed on top of the supporting polyethylene substrate. The outer dimension of the proposed antenna is $W_{\text{total}} = 7.5$ mm and $L_{\text{total}} = 88$ mm, while the internal slot length is $W_{\text{slot}} = 1.5$ mm and $L_{\text{slot}} = 68$ mm.

Once the antenna impedance was properly tuned for the best complex conjugate matching at 870 MHz, the power transmission coefficient τ between the antenna and the RFID tag was calculated from the simulated input impedance Z_a according to

$$\tau = \frac{4R_a R_c}{|Z_a + Z_c|^2} \tag{1}$$

where $Z_a = R_a + jX_a$ and $Z_c = R_c + jX_c$ is the simulated antenna input impedance and the microchip characteristic
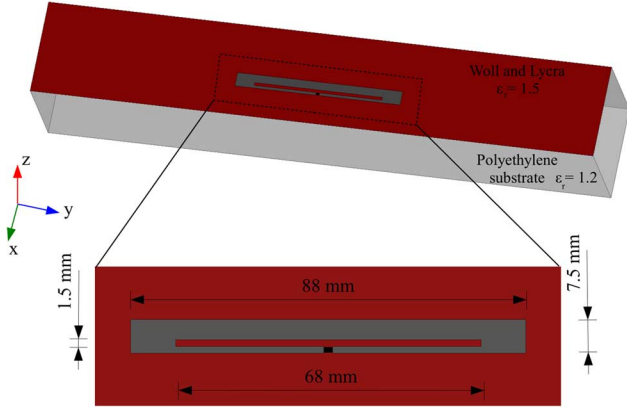
Fig. 2. 3D Simulation model of the proposed wearable RFID sensor. The substrate characteristics were defined based on the dielectric measurements reported in Table I. As an RF excitation, a lumped port was set according to the RFID tag impedance $Z_c = 25 - j200\ \Omega$.

impedance given in Table II, respectively. Next, the return loss, or S_{11}, can be calculated by [9]

$$S_{11} = 20 \log_{10}(1 - \tau). \tag{2}$$

The equation editor in HFSS allows for a convenient real time plotting of this custom output quantity.

In Fig. 3(a) we show the simulation of the antenna's input impedance Z_a. At the desired center frequency of 870 MHz, the complex impedance is equal to $Z_a = 57.1 + j180.2$. The return loss S_{11}, computed with (2), is depicted in Fig. 3(b) for the same frequency sweep. We note that the real part of the input impedance is higher than expected. This deviation is due to the final-tuning performed for matching the sheet impedance to the actual measured prototype. As a result, the simulated input impedance is a contribution of both the antenna geometry and the complex sheet impedance used to model the conductive textile. However, the S_{11} shows a good level of matching, with a very small percentage of power reflected in band: 0.04–0.1%. The 10 dB return loss bandwidth is about 70 MHz, covering with good impedance matching the RFID chip frequency band from 870 to 915 MHz. The relevant Industrial Scientific and Medical band (ISM) is 865–928 MHz.

The radiation characteristic resembles the same omnidirectional beam as a conventional dipole radiator. As shown in Fig. 4, the maximum current intensity occurs along the two major edges, while it reaches lower intensity along the short edges. The resulting beam will therefore be characterized by a uniform radiation around the plane normal to the feed port ($x - z$ plane) and two nulls along the major axis ($y - z$ plane). In Fig. 4 we show the 3D beam with respect to the antenna layout. The maximum gain is about 0.8 dBi, which is lower with respect to a copper-based design, due to the textile complex sheet impedance.

III. EXPERIMENTAL RESULTS

When designing knitted antennas, the transition between the theoretical model to the actual prototype requires some iterations to accomplish the desired layout. While the theoretical di-
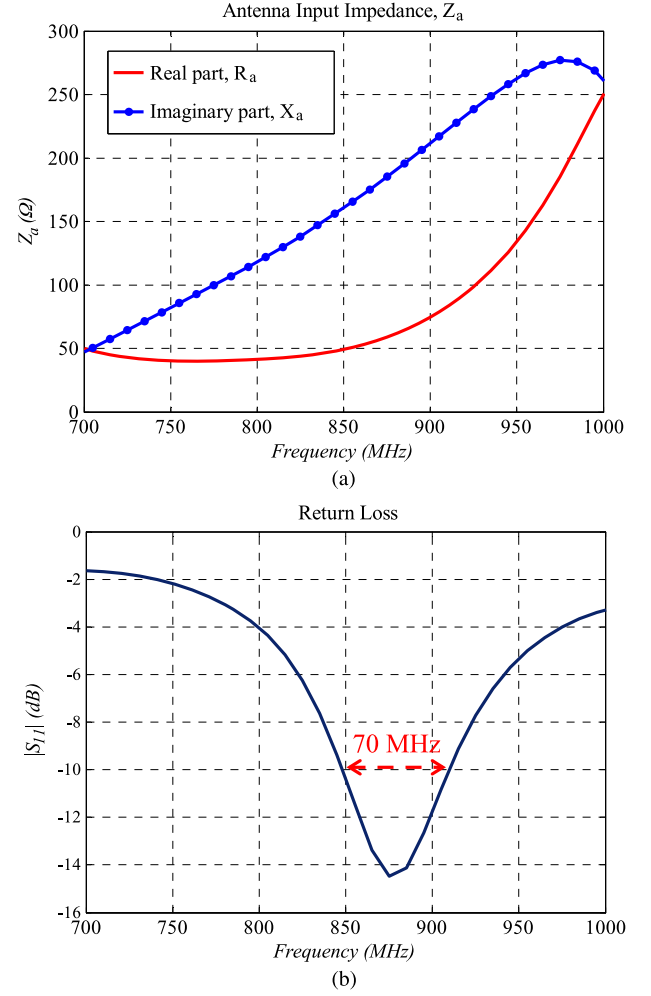

(a)

(b)

Fig. 3. Simulated antenna input impedance. (a) Simulated real and imaginary parts of antenna input impedance. (b) Numerical estimation of the return loss S_{11} using (2). The antenna layout has been optimized to yield good impedance matching within the whole frequency range of the RFID tag: 870–915 MHz.
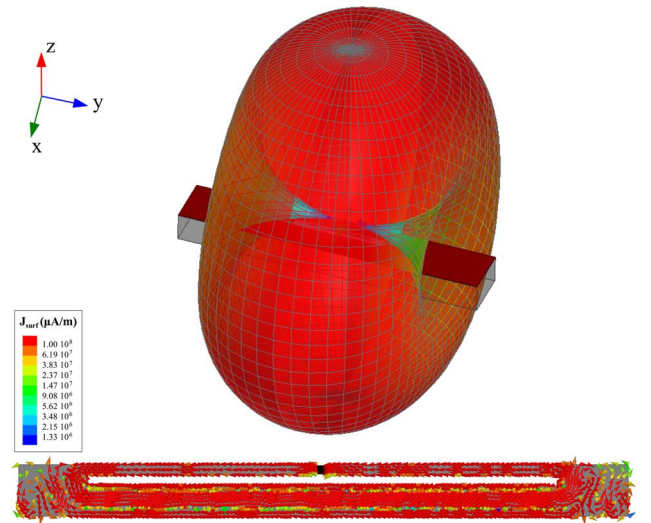

Fig. 4. Simulated current distribution and radiation characteristics. The highest density of current distribution flows along the major axis, generating an omnidirectional beam normal to the y axis.

mensions are given in the metric units, the CAD software used for knitting machines defines the layout in terms of the number
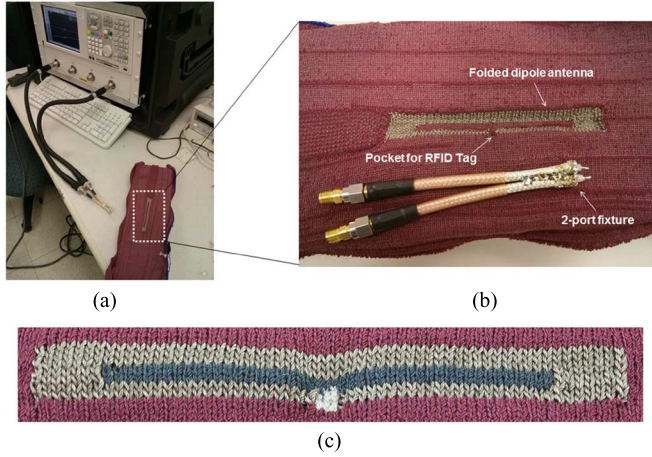
Fig. 5. Experiment setup of S-parameters measurements. (a) Network analyzer with detail of the two-port fixture for balanced impedance measurements. (b) Knitted dipole antenna prototype with detail of the pocket for RFID tag housing. (c) Close-up picture of the knitted pattern.
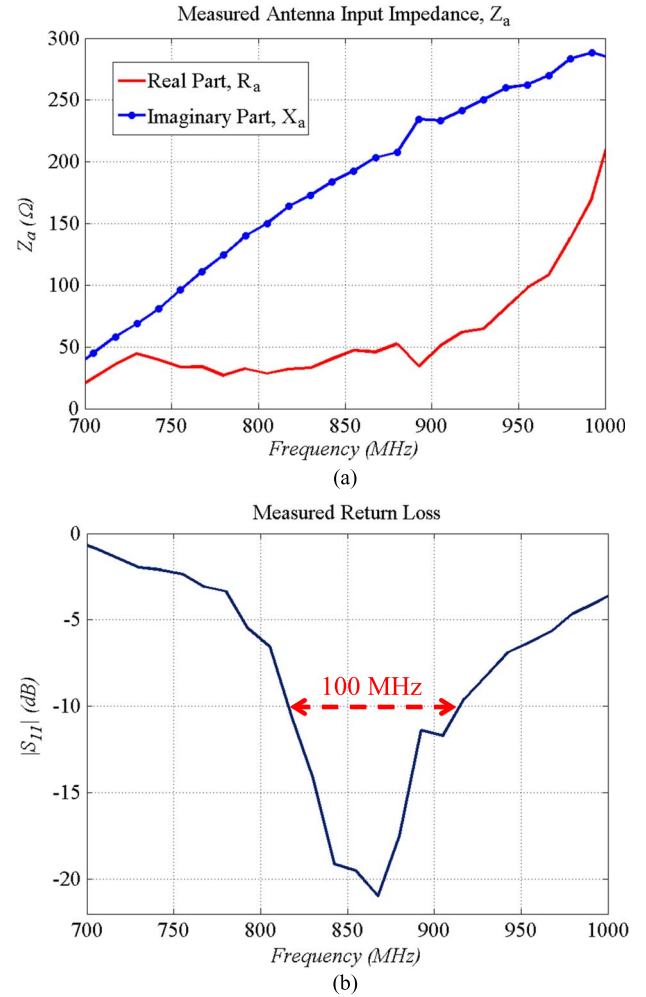

Fig. 6. Measured antenna input impedance. (a) Real and imaginary parts of input impedance using the differential measurement approach. (b) Extraction of the return loss S_{11} using (2). The 10 dB return loss bandwidth is 100 MHz.

of yarns and loops. Once the desired knitted folded antenna was manufactured, its input impedance and radiation pattern were characterized and compared to the expected numerical results.

A. Input Impedance Measurements

The topology of folded dipole antennas is characterized by balanced input impedance, while the conventional coaxial lines are unbalanced (quasi-TEM). This characteristic does not allow for conventional scattering parameters (S-parameters) characterization using the coaxial ports of a network analyzer. However, the antenna's input impedance can still be determined through a differential approach, with a proper coaxial fixture that considers the antenna to be a two-port network. Fig. 5 shows the experiment setup with network analyzer and two-port fixture, along with the prototype of the knitted folded dipole antenna.

In these measurements, the fixture was made by two $\lambda/4$ semi-rigid coaxial cables terminated with SMA connectors at one end. The two cables were aligned together by soldering the outer shields and the central conductors were connected to the knitted antenna by using conductive epoxy. The network analyzer was properly calibrated and the fixture's length de-embedded through the port-extension function.

The measured two-port complex S-parameters were loaded into MATLAB for computing the antenna impedance Z_a through the following expression [10]:

$$Z_a = R_a + j\,X_a = 2\,Z_0 \frac{(1 - S_{11}^2 + S_{21}^2 - 2S_{12})}{(1 - S_{11})^2 - S_{21}^2} \quad (3)$$

where Z_0 is the 50 Ω characteristic impedance of the network analyzer. The antenna can reasonably be assumed to be symmetrically balanced, therefore in (3) we assume $S_{11} = S_{22}$ and $S_{12} = S_{21}$. After determining the antenna's impedance Z_a, the return loss S_{11} was calculated using (2).

In Fig. 6(a) the measurements show that at the desired center frequency of 870 MHz, the impedance is equal to $Z_a = 49.5 + j205.0\ \Omega$, which yield a good conjugate matching with the RFID tag impedance Z_c. The respective return loss in Fig. 6(b) exhibits a 10 dB bandwidth of 100 MHz, covering the desired frequency range. Through comparison with the simulated return loss, we notice that the measurement returns a larger 10 dB bandwidth. This is potentially due to the lower Q factor of the manufactured knitted radiator, which tends to be more lossy, which in turn yields a larger bandwidth.

Generally speaking, the Q factor is the ratio between the energy stored in the reactive field and the energy radiated. Its value is determined by the conductor thickness, and the conduction losses are proportional to the conductor thickness. A higher conductor thickness leads to higher conduction losses, lower Q and thus larger bandwidth. For modeling the conductive textile we used a 2D complex sheet impedance, but the actual prototype presents a finite textile thickness for which this planar model cannot account. As a verification, we re-simulated the antenna assuming a higher resistive part of the sheet impedance Z_S. We have seen that for every 0.05 Ω of incremental value of $\mathrm{Re}\{Z_S\}$
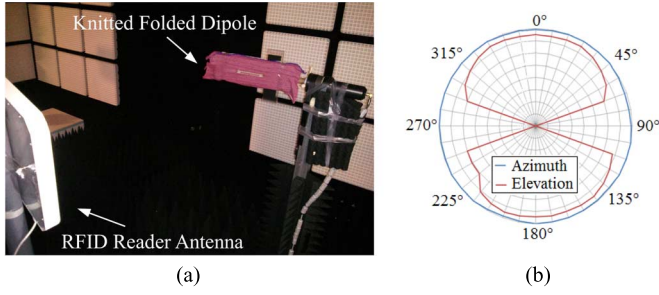
Fig. 7. Anechoic chamber setup for radiation pattern measurements. (a) Directional antenna connected to Impinj Speedway reader and knitted folded dipole antenna with MAGICSTRAP tag attached to the 3D manipulator. (b) Resulting radiation pattern.

Fig. 8. Return loss of the RFID tag antenna for different distances d from the human stomach model.

the bandwidth increases by approximately 15%, but at the same time the resonant frequency is shifted slightly upward. Therefore, the complex sheet impedance is a very useful tool for modeling textile RF structures, but it also shows some trade-offs between resonant frequency and bandwidth due to the lack of a third dimension (thickness). Fortunately, the UHF RFID frequency band (860–915 MHz) is relatively narrow and both the simulated and the measured S_{11} cover the entire bandwidth with good impedance matching.

B. Radiation Pattern Measurement

Evaluating the directivity of the knitted antenna allows us to infer the current distribution occurring along the conductive threads. To this end, the knitted folded dipole prototype equipped with the MAGICSTRAP RFID tag, and an Impinj Speedway reader [12], were set 70 cm apart within an anechoic chamber. The antenna was attached to a 3D manipulator for azimuth and elevation plane rotations. The rotations occurred in steps of 5°, and 200 RSSI values were averaged for each angular step. Fig. 7 shows the anechoic chamber setup along with the resulting azimuth and elevation planes. The knitted folded dipole antenna offers the expected omnidirectional radiation in the elevation plane, and the two nulls in the azimuth plane correspond to the location of the antenna's short edges. This is in good agreement with the predicted radiation characteristics of Fig. 4. The high conductive thread density along the longer edges allows us to support the expected current flow and generation of the desired radiation pattern.

C. Consideration on the Human Body Proximity

The proposed wearable RFID strain sensor aims to determine human functions such as breathing/contraction patterns or limb movements. Therefore, it is important to evaluate human body effects on antenna performance due to the absorption of radiation between tissue layers.

HFSS along with the 3D human body model [11], were used to simulate the antenna at different heights above the human stomach to determine loading effects. We observed that the resonant frequency is progressively downshifted and attenuated when the sensor approaches the human skin. As shown in Fig. 8, at the center frequency of 870 MHz, the S_{11} falls below the -6 dB threshold when the distance is between 5 mm $< d <$ 10 mm. However, the optimal S_{11} regime under -10 dB is
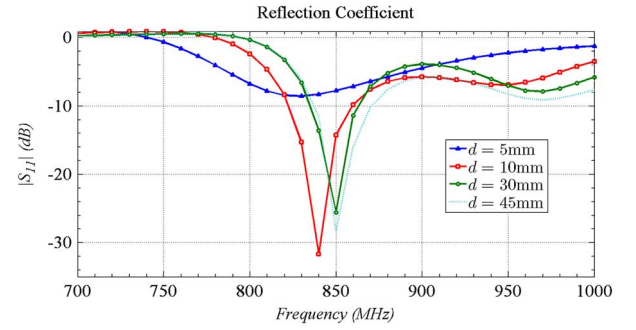

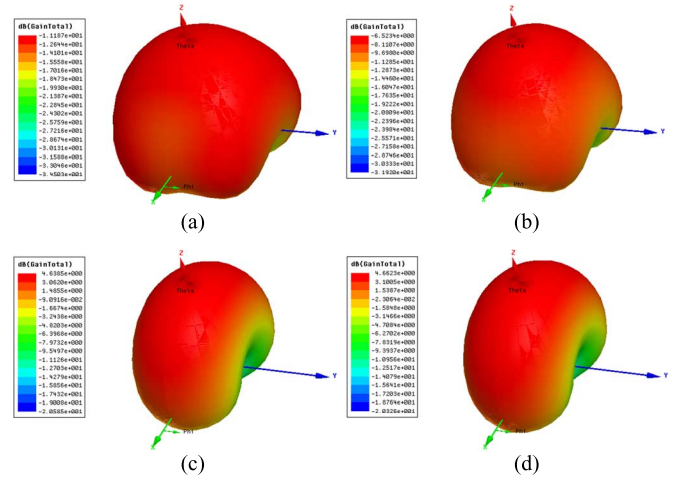Fig. 9. Radiation patterns as function of the heights d above the human chest, at the frequency of 870 MHz. (a) $d = 5$ mm. (b) $d = 10$ mm. (c) $d = 30$ mm. (d) $d = 45$ mm. Under low distance the gains are negative, while when d is increased, the gains are about 60% higher than without human chest.

achieved when $d > 45$ mm. This analysis allows for performance optimization under these loading effects. In fact, the antenna can be tuned to resonate 30–40 MHz above the desired center frequency and a fabric spacer of 5–10 mm can be added behind it in order to maintain good impedance matching when worn.

The radiation pattern also changed significantly in the proximity of the human body. Because of absorption and reflection of the tissue layers, the radiation is directed broadside, normal to the antenna's plane. As depicted in Fig. 9, when the distance d is less than 10 mm, the antenna's efficiency degrades significantly, causing negative gains. When $d > 10$ mm the antenna exhibits directional beams with positive gain, up to 3.4 dBi. The Half-Power Beamwidth (HPBW) is comparable to the omnidirectional beam showed in Fig. 4. Non-conductive fabric spacers can be knitted with the final garment for achieving the desired distance between the antenna and the skin.

If the antenna becomes wet due to sweat the functionality of the sensor would be altered due to the conductive characteristic of water. For this reason, the fabric spacer mentioned above will also act as a protective padded layer keeping the antenna away from the skin. This additional layer would protect the sensor preserving the elasticity of the antenna.

IV. APPLICATION AS A WEARABLE BREATHING MONITOR

Since the aim of this sensor is to capture contractions or respiration of a human body, we have performed a preliminary strain sensing analysis using a medical mannequin used for medical training. Specifically, we focused our attention to the application of the sensor as a breathing monitoring system.

Monitoring if a child is breathing regularly can be helpful in detecting apnea with the possibility to prevent an acute cardiorespiratory arrest. Currently, wearable baby monitors are made from a baby onesie equipped with a WiFi or Bluetooth module that collects data from sensors that are integrated into the garment, and sends the data to a mobile device [2]. However, these monitors employ active modules that are bulky and need to be recharged regularly. The wearable strain sensor described in this section has the potential of improving this current technology since it can be used to detect the breathing pattern of a child through a more comfortable, and fully textile garment that does not require batteries or cumbersome electronics.

A. Experiment System Setup

In order to evaluate the performance of the strain sensor for respiration monitoring, we have used a mechanical baby mannequin, which is used for medical training, for testing the device. This mannequin, called Laerdal SimBaby [13], can be programmed with specific breathing and non-breathing intervals and the chest of the baby resembles the usual expansion of a breathing pattern. The wearable strain sensor was fitted around the baby mannequin's chest, and the Impinj Speedway RFID reader [12] was placed at about 1 m from the mannequin. The minimum distance required by the FCC is 20 cm [19]. Five minutes of continuous data was collected from the programmable infant mannequin device as follows: breathing from 0–60 seconds, non-breathing from 60–100 seconds, breathing from 100–210 seconds, non-breathing from 210–240 seconds, breathing from 240–300 seconds. To remove noise and mitigate quantization, a Gaussian filter was applied to the RFID data collected. The algorithm considered for determining activity state is the Support Vector Machine (SVM) [14]. This algorithm is a machine learning model that analyzes data to recognize patterns used for classification analysis. This analysis separates the data points collected by the RFID interrogator into two classes: in this case, breathing and non-breathing classes. The data points are arranged into a 2D plot with standard deviation on the x-axis and RSSI mean on the y-axis. In Fig. 10, the experimental system setup comprising the SimBaby mannequin and controlling system, along with the proposed wearable sensor and the RFID interrogator are shown. The $G_{tx} = 6$ dBi interrogator antenna is placed at $d = 1$ m from the simbaby. The RFID reader output power is set to $P_{out} = 30$ dBm to comply with the maximum EIRP power of 36 dBm as specified by the FCC Part 15.247 regulations. The power density at the simbaby position can be calculated as

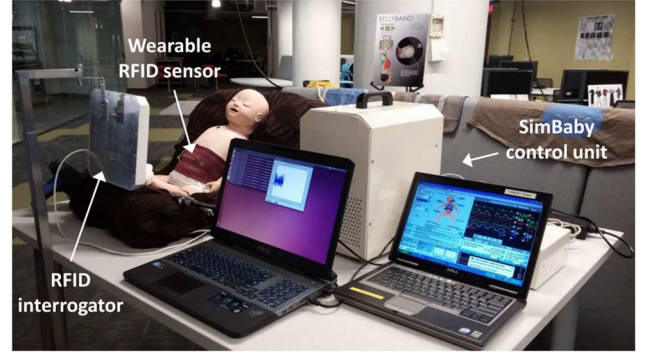$$P_d = \frac{P_{out}G_{tx}}{4\pi d^2} = 0.03 \text{ mW/cm}^2. \qquad (4)$$

Fig. 10. Experimental setup for baby breathing monitoring. The SimBaby mannequin is controlled by a programmable actuator that expands the baby's chest with specific breathing rates. The wearable RFID sensor, worn around the baby's chest, is interrogated by the RFID unit in front of it.

The effective area of the wearable sensor is $A_e = 88$ mm $\times$ 7.5 mm as shown in Fig. 2. Therefore, the power received from the wearable sensor is

$$P_r = P_d A_e = 0.22 \text{ mW}. \qquad (5)$$

Since the impedance match between the RFID tag and the antenna is relatively high we can assume ideal efficiency, which means that the back-scattered power equals the received power. The gain of the wearable RFID sensor is $G_{sensor} = 0.8$ dBi, which yield an Equivalent Isotopically Radiated Power of

$$EIRP = P_r G_{sensor} = 0.26 \text{ mW}. \qquad (6)$$

B. Experimental Results

To classify the data into breathing and non-breathing states, the statistical features of windows of data points are arranged into R^n space, and a line, curve, or plane is computed that "best" divides the points. There can be many ways to separate the data, and there can be no possible way to cleanly separate the data if the data points are not well-separable. The degree of separability of data points into classes is provided by metrics, such as the Fisher Linear Discriminant ratio function (FDR) [15], which was employed for this study using mean μ and standard deviation δ and defined as follows:

$$\text{FDR} = \frac{(\mu_1 - \mu_2)^2}{(\delta_1^2 + \delta_2^2)}. \qquad (7)$$

Using this method, it was found that, when arranging the RSSI values collected into temporal windows, the mean and standard deviation of the data within each window yield well-separable features, which was confirmed by the performance of our experimental study, discussed later in this section. Because the mean and standard deviation were found to be highly separable, they plot in such a way that one or more separating "lines" can be drawn that separates most of the data points. The "best" such separating line is the one that separates the groups of points and also maximizes the distance or margin between the line and the

nearest data point from each class. This way, new data points can be classified with a low risk of error due to conflating the two states by virtue of the separating line being drawn too closely to the boundary of either class. Other data elements, such as the Doppler and phase angle from the RFID interrogator, were considered, as well as other statistical features of the RSSI, but these were not predicted by the FDR to be as linearly separable and thus not predicted to be conducive to real-time predictive analysis.

To determine the separability of features via the FDR metric, it is necessary to compute features on windows of both breathing and non-breathing classes of data. It is not possible to collect training data in the non-breathing class, since the test subject would have to cease respiratory activity for purposes of data training, though this is feasible in simulation for purposes of determining which features are most suitable for deployment. In other applications, such as uterine monitoring or motion monitoring, training is feasible in both classes, so Two-Class analysis remains valuable; however, results from Two-Class classifiers are compared against single-class anomaly detectors in order to compare the performance of a single-class approach when it is needed.

Using the mean and standard deviation as the base features in this study, the FDR was computed across the same simulated data but with different window sizes: 128, 64, 32, and 16-element windows. For the approximately 30 Hz RFID interrogator being used, this corresponds to time windows of 4.27, 2.13, 1.07, and 0.53 seconds, respectively. Experimental results have shown that the FDR separability improves as the window size increases, as shown in Fig. 11.

Some related efforts do exist that did not indicate detection time or real-time detection accuracy. However, like our work, it is noted that improved signal to noise performance is observed when the window size is increased [22]. Two measurements are taken on the chest wall and the abdomen, and the phases of the sinusoidal signals are compared to classify breathing state. We are using statistical features of a single placement currently in order to measure detection accuracy against known conditions (pre-programmed into the SimBaby), but a second chip placement on the body is feasible on the proposed textile band. A feature window length of 10-seconds was identified in another work, which is approximately what we have found to yield optimal results as well [23]; this work utilizes the ECG signal as opposed to our passive RFID, and assuming similar detection accuracies, a passive RFID signal appears to be a viable alternative.

Using this information, a web service was written to interrogate the RFID tag and gather raw data about its state, including its RSSI value. Initially, this service runs on the interrogator prior to any statistical inference, so that several seconds of training data can be obtained in order to establish a baseline of the window features under normal conditions for the subject. For example, the subject may breathe normally during this time, and the web service will store the statistical features corresponding to that state during the training phase. This web service is queried by a client periodically to classify subject state from windows of that data. This service computes whether the current window's features lie on the normal (breathing) or
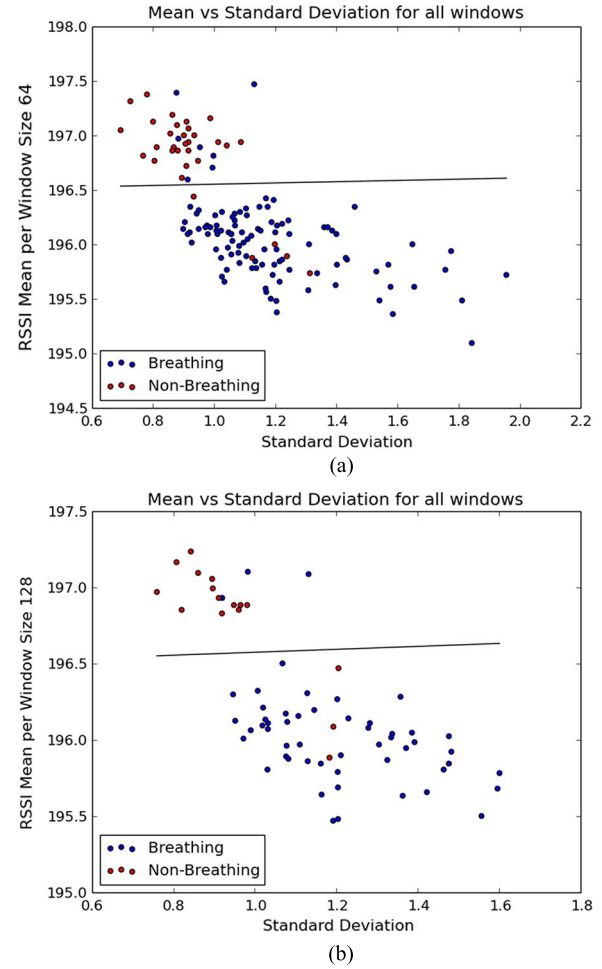

Fig. 11. Experimental results of the breathing monitoring test. The support vector machine has been used to separate the breathing and non-breathing patterns from the collected RSSI data. (a) Plot generated using a window size of 64. (b) Plot generated using a window size of 128. The larger window size allows a better separation of the two clusters.

non-normal (non-breathing) side of the support vector space computed during training. Additionally, it runs a hypothesis test to determine whether this window's data is likely comprised only of zero-mean noise, indicating a non-breathing state. This additional information can help augment in cases when the support vector computation lies within the margin or close to the boundary separating the breathing and non-breathing classes. Other biological data classification efforts have used statistical features such as the mean, standard deviation, kurtosis, and others [18]; the features chosen for this study, based on the separability predicted by the FDR, include the window mean, window standard deviation, and the p-value of the t-test using a 0-mean window hypothesis. Varying the window size and training set size, as well as utilization of hypothesis testing results to inform the support vector machine improves classification accuracy to approximately 77% in this study. These services were deployed in a real-time monitoring prototype that detected breathing cessation in 8 seconds, and a restoration of breathing in 5 seconds.

The results shown in Fig. 11 show that the wearable RFID sensor along with the Support Vector Machine algorithm

separates the breathing and non-breathing patterns. The horizontal separation of points in the breathing and non-breathing classes indicates that the RSSI window mean better informs the state prediction of the subject, due to the overlap between the standard deviation of windows across both classes. Although the RSSI standard deviation feature is somewhat separable, it yields more overlap than the RSSI mean. This is visualized as the upward-sloping separating line in Fig. 11, and results from the misclassified points "pulling" the line upwards towards those points. As a result, this feature is not conducive to a hyperplane approach such as a support vector machine like the mean, and instead is more conducive for use in an ensemble approach using nearest neighbor or k-means clustering, which is the subject of our current work. The few points that belong to the wrong cluster are errors due to the mannequin transitioning from breathing to non-breathing states, and vice versa.

V. CONCLUSION

In this paper we discussed the design and application of a knitted folded dipole antenna equipped with an inductively coupled RFID chip for the development of a wireless, wearable sensor. The aim of the knitted passive sensor is for monitoring respirators or other body movements through a comfortable and battery-less wireless sensor. The unique feature of this work is the development of knitted antennas embedded in the host garment and equipped with inductively-coupled RFID tags for backscatter power sensing. We developed statistical analysis and signal processing algorithms to interpret and classify this data to determine the wearer's state. Through the use of commercially available RFID readers, the wearable RFID sensor responds to mechanical deformations with backscattered power variations (RSSI). The successive filtering and analysis allows inference about the biomedical parameter that is being monitored.

For developing this sensor, first we have designed and tested a folded dipole antenna tuned for impedance matching with an inductively coupled RFID tag. Specifically, we have applied the complex sheet impedance numerical condition in order to account for the actual losses and parasitic effects introduced by the knitted conductive yarns. The input impedance measurements showed good agreement with the numerical simulation, and the radiation pattern resembles the predicted directivity typical of a dipole antenna.

Second, we have performed an experiment for validating the sensor as a wearable breathing monitor. A programmable medical baby mannequin has been set with specific breathing and non-breathing intervals, with the chest of the baby expanding as an actual breathing movement. The wearable strain sensor was fitted around the baby's chest, and a commercial RFID reader was used to collect the RSSI data. Next, a machine learning technique has been used for post-processing the data and it has shown that the two breathing and non-breathing patterns can be successfully separated.

According to the results of this work, we demonstrated that fully knitted antennas equipped with inductively coupled RFID tags provide good strain sensing performance to be used as wireless sensors for monitoring biomedical parameters.

REFERENCES

[1] OM Signal [Online]. Available: http://www.omsignal.com
[2] The Mimo Smart Baby Monitor [Online]. Available: http://www.mimobaby.com
[3] C. Occhiuzzi, C. Paggi, and G. Marrocco, "Passive RFID strain-sensor based on meander-line antennas," *IEEE Trans. Antennas Propag.*, vol. 59, no. 12, pp. 4836–4840, 2011.
[4] D. Cottet, J. Grzyb, T. Kirstein, and G. Troster, "Electrical characterization of textile transmission lines," *IEEE Trans. Adv. Packag.*, vol. 26, no. 2, pp. 182–190, 2003.
[5] D. L. Paul, M. Klemm, C. J. Railton, and J. P. McGeehan, "Textile broad-band E-patch antenna at ISM band," in *Proc. IET Seminar Ant. and Propag. For Body-Centric Wireless Communications*, 2007.
[6] I. Locher, M. Klemm, T. Kirstein, and G. Troster, "Design and characterization of purely textile patch antennas," *IEEE Trans. Adv. Packag.*, vol. 29, no. 4, pp. 777–788, 2009.
[7] Murata MAGICSTRAP UHF Tag [Online]. Available: http://www.murata.com/en-us/campaign/ads/americas/rfid
[8] K. Koski, A. Vena, L. Sydanheimo, L. Ukkonen, and Y. Rahmat-Samii, "Design and implementation of electro-textile ground planes for wearable UHF RFID patch tag antennas," *IEEE Antennas Wireless Propag. Lett.*, vol. 12, no. 1, pp. 964–967, 2008.
[9] T. Koskinen and Rahmat-Samii, "Metal-mountable microchip RFID tag antenna for high impedance microchip," in *Proc. IEEE Eur. Conf. Ant. and Propag.*, 2009.
[10] Q. Xianming, C. K. Goh, and Z. N. Chen, "Impedance characterization of RFID tag antennas and applications in tag co-design," *IEEE Trans. Microw. Theory Tech.*, vol. 57, no. 5, pp. 1268–1274, 2009.
[11] Ansys 3D Human Body Model [Online]. Available: http://www.ansys.com
[12] Impinj Speedway Reader [Online]. Available: http://www.impinj.com/products/readers/
[13] Laerdal SimBaby Infant Patient Simulator [Online]. Available: http://www.laerdal.com/us/SimBaby
[14] C. Corinna and V. Vapnik, "Support-vector networks," *Machine Learn. J.*, vol. 30, no. 3, 1995.
[15] R. A. Fisher, "The use of multiple measurements in taxonomic problems," *Ann. Eugenics*, vol. 2, pp. 179–188, 1936.
[16] J. B. MacQueen, "Some methods for classification and analysis of multivariate observations," in *Proc. Berkeley Symp. Mathematical Statistics and Probability*, 1967.
[17] B. Moslem, M. O. Diab, M. Khalil, and C. Marque, "Combining data fusion with multiresolution analysis for improving the classification accuracy of uterine EMG signals," *EURASIP J. Adv. Signal Process.*, 2012, 2012:167.
[18] G. Thatte, M. Li, S. Lee, B. A. Emken, M. Annavaram, S. Narayanan, and U. Mitra, "Optimal time-resource allocation for energy-efficient physical activity detection," *IEEE Trans. Signal Process.*, vol. 59, no. 4, pp. 1843–1857, 2011, 10.1109/TSP.2010.2104144.
[19] FCC Review of RF Exposure Policies [Online]. Available: https://www.fcc.gov/document/fcc-review-rf-exposure-policies
[20] D. Zito, D. Pepe, M. Mincica, F. Zito, A. Tognetti, A. Lanata, and D. De Rossi, "SoC CMOS UWB pulse radar sensor for contactless respiratory rate monitoring," *IEEE Trans. Biomed. Circuits Syst.*, vol. 5, no. 6, pp. 503–510, Dec. 2011.
[21] J. Jin and E. Sanchez-Sinencio, "A home sleep apnea screening device with time-domain signal processing and autonomous scoring capability," *IEEE Trans. Biomed. Circuits Syst.*, vol. 9, no. 1, pp. 96–104, Feb. 2015.
[22] D. Falie, L. David, and M. Ichim, "Statistical algorithm for detection and screening sleep apnea," in *Proc. Int. Symp. Signals, Circuits and Systems*, Jul. 9–10, 2009, pp. 1–4.
[23] L. Mirmohamadsadeghi, S. Fallet, A. Buttu, J. Saugy, T. Rupp, R. Heinzer, J.-M. Vesin, and G. P. Millet, "Sleep apnea detection using features from the respiration and the ecg recorded with smart-shirts," in *Proc. IEEE Biomedical Circuits and Systems Conf.*, Oct. 22–24, 2014, pp. 61–64.

Damiano Patron (S'11–M'15) received the B.S. degree in electronics engineering from the University of Padua, Padua, Italy, in 2010, and the M.S. and Ph.D. degrees in electrical and computer engineering from Drexel University, Philadelphia, PA, USA, in 2013 and 2015, respectively.

From 2002 to 2010, he worked with Euro-Link S.r.l. as a System Integrator of RFID Systems. In 2010, he joined the start-up company Adant Inc. as an RF and Antenna Engineer, designing reconfigurable antennas for WiFi and RFID applications. Currently, he is working as a Staff Scientist for Witricity Corporation on new wireless charging technologies. His Ph.D. research focused on the design of reconfigurable antennas for throughput maximization and DoA estimation in wireless networks. He also worked on the development of wearable sensors and power harvesting systems. He is the author and coauthor of several patents, and scientific papers in the field of reconfigurable antennas, antennas miniaturization and wearable technologies.

Dr. Patron received several awards, including the Young Scientist Best Paper Award at the ICEAA IEEE APWC EMS Conference in 2013, and the first prize for the Rectenna Spinout Contest at the 9th Annual IEEE International Conference on RFID in 2015.

William Mongan (M'05) received the B.S. and M.S. degrees in computer science, and the M.S. degree in science of instruction from Drexel University, Philadelphia, PA, USA, in 2005, 2008, and 2008, respectively.

From 2003 to 2008, he was a Researcher in the Software Engineering Research Group (SERG) at Drexel University, where he worked in program comprehension and service-oriented architectures. He serves as an Associate Teaching Professor and Associate Department Head for Undergraduate Affairs in the Department of Computer Science at Drexel University, where his research focus is signal processing and data analytics on real-time biofeedback.

Mr. Mongan is a Senior Member of the Association for Computing Machinery (ACM).

Timothy P. Kurzweg (S'92–M'95–SM'09) received the B.S. degree from Pennsylvania State University, University Park, PA, USA, in 1994, and the M.S. and Ph.D. degrees from the University of Pittsburgh, Pittsburgh, PA, USA, in 1997 and 2002, respectively, all in electrical engineering.

Currently, he is an Associate Professor in the Department of Electrical and Computer Engineering, Drexel University, Philadelphia, PA, USA. His research interests include programmable imaging with optical MEMS, precancerous detection using white-light spectroscopy, diffuse optical communication using space-time coding, and non-traditional electronics and antennas.

Dr. Kurzweg is a member of the IEEE Lasers and Electro-Optics Society, the International Society for Optical Engineers, and the Optical Society of America.

Adam Fontecchio (SM'11) received the B.A., M.Sc., and Ph.D. degrees in physics from Brown University, Providence, RI, in 1996, 1998, and 2002, respectively.

Currently, he is a Professor in the Electrical and Computer Engineering Department, Drexel University, Philadelphia, PA, USA, and is Vice-Dean of the Graduate College. He is the inaugural Director of the Center for the Advancement of STEM Teaching and Learning Excellence (CASTLE), serving as Vice-Chair of the IEEE Philadelphia Section, and is a member of the IEEE-USA K-12 STEM Literacy Committee. His research focuses on the area of nanophotonics. He has served as PI or Co-PI on more than $18 million in sponsored research funding, and has authored over 90 peer-reviewed papers.

Dr. Fontecchio was selected as the 2015 Delaware Valley Engineer of the Year. He was also the recipient of a NASA New Investigator Award, the Drexel Graduate Student Association Outstanding Mentor Award, the Drexel University ECE Outstanding Research Achievement Award, and the International Liquid Crystal Society Multimedia Prize.

Genevieve Dion received the B.A. degree in industrial arts from San Francisco State University, San Francisco, CA, USA, and the Master of Industrial Design degree from University of the Arts, Philadelphia, PA, USA.

Currently, she is an Associate Professor in the Department of Design at the Westphal College of Media Arts and Design, Drexel University, Philadelphia, PA, USA. Her research uses advanced manufacturing processes for the flexible production of mass-customizable smart textiles, including the development of seamlessly knitted electronic yarns into "Garment Devices." She believes that design plays an important role at the onset of the scientific process and brings this unique approach to her multidisciplinary research laboratory. During her tenure at Drexel University, she spearheaded interdisciplinary research projects utilizing digital knitting machines as research tools. In 2012, she founded the Shima Seiki Haute Tech Lab at the ExCITe Center. Her work on permanently pleated silk has been in the collections of the Victoria and Albert Museum in London (2003) and the DeYoung Museum in San Francisco (2010). She is an advisor to an NSF Fellow in Materials Science and advised a former Department of Defense Fellow in Materials Science.

Ms. Dion was named one of Fast Company's MCP1000 and Top 100 Most Creative People in Business in 2014. She was appointed as "Innovation Ambassador" to the United Nations' World Summit on Innovation & Entrepreneurship.

Endla K. Anday received the Medical Degree from the Medical College of Pennsylvania, Philadelphia, PA, USA, in 1973.

She completed a residency in Pediatrics at the Children's Hospital of Philadelphia in 1975 and Fellowship training in Neonatal-Perinatal Medicine in 1978. Following a year of fellowship in pulmonary physiology in the Department of Physiology, University of Pennsylvania, Philadelphia, she was appointed Assistant Professor of Pediatrics in the Department of Pediatrics at the Children's Hospital of Philadelphia, University of Pennsylvania School of Medicine, Section of Neonatal-Perinatal Medicine. In addition to clinical medicine, she received numerous grants to investigate the mechanisms of brain injury following hypoxic-ischemic insults, effect of cocaine in the brain of a neonatal animal model and the effect of maternal high fat diet in the fetus on the development of adult-onset metabolic syndrome. She participated in a number of national clinical trials, including the effect of exogenous surfactant on the lung of the premature newborn, the effect of thyroid-stimulating hormone on lung biochemical maturation, the efficacy, safety and tolerance of oral Zidovudine (ZDV) in HIV-infected pregnant women and their infants and the efficacy of recombinant human granulocyte-macrophage colony stimulating factor for prophylaxis of neonatal nosocomial infection. In 1996, she was recruited to St. Christopher's Hospital for Children in the role of Regional Clinical Director for Neonatal Services. She was appointed to Professor of Pediatrics and currently serves as the Medical Director of the Neonatal Intensive Care Unit at Hahnemann University Hospital, Philadelphia. She has more than 80 first author papers and chapters in books.

Dr. Anday has served on numerous committees in the Academy of Pediatrics, Section of Neonatal-Perinatal Medicine and is on the Editorial Board of the NeoReviewsPlus. She was selected for "Best Doctors in America" and "Top Pediatricians in America" and holds membership in several prestigious societies including: Society for Pediatric Research, American Pediatric Society, The New York Academy of Sciences, and Society for Gynecologic Investigation. She is also a member of the Sigma Xi Society, Alpha Omega Alpha.

Kapil R. Dandekar (S'95–M'01–SM'07) received the B.S. degree in electrical engineering from the University of Virginia, Charlottesville, VA, USA, in 1997, and the M.S. and Ph.D. degrees in electrical and computer engineering from the University of Texas at Austin, Austin, TX, USA, in 1998 and 2001, respectively.

He worked at the U.S. Naval Observatory in 1992 and at the U.S. Naval Research Laboratory from 1993–1997. In 2001, he joined the Electrical and Computer Engineering Department at Drexel University, Philadelphia, PA, USA. Currently at Drexel University, he is a Professor in Electrical and Computer Engineering; the Director of the Drexel Wireless Systems Laboratory (DWSL); and Associate Dean for Research and Graduate Studies in the Drexel University College of Engineering. DWSL has been supported by the U.S. National Science Foundation, Army CERDEC, National Security Agency, Office of Naval Research, and private industry. His research interests and publications involve wireless, ultrasonic, and optical communications, reconfigurable antennas, and smart textiles. Intellectual property from DWSL has been licensed by external companies for commercialization.

Dr. Dandekar is a former member of the IEEE Educational Activities Board and cofounder of the EPICS-in-IEEE program.